Introduction

Waveform inversion (WI) builds velocity models using seismic wavefields (Tarantola, 1984; Woodward, 1992; Pratt, 1999; Sirgue and Pratt, 2004; Plessix, 2006; Vigh and Starr, 2008; Plessix, 2009; Symes, 2009). Although costly, this methodology is gaining momentum due to its accuracy and due to its potential for robust model updates in complex geology. This method requires accurate wavefields simulated using a wave-equation, usually constant-density acoustic. The technique also employs an objective function (OF) which captures the similarity between simulated and observed seismic wavefields. Though commonly overlooked, WI can also be implemented in the image-domain, which requires a modest alteration of the OF definition when considering multiple seismic experiments (Symes, 2009; Yang and Sava, 2011).

Both data- and image-domain implementations have weaknesses which degrade their effectiveness. For the data-domain implementation, we assume that we can accurately simulate the physics of wave propagation, which is difficult when the earth is characterized by strong (poro)elastic effects. For the image-domain implementation, we assume that the migrated images are perfectly focused when the model is correct, which is not the case in areas of poor illumination, e.g. sub-salt. Here we concentrate on the image-domain WI, sometimes known as wavefield tomography (WT). We describe a method for illumination compensation which increases the robustness of WT in areas of poor illumination.

Theory

An effective gradient calculation uses the adjoint state method (Plessix, 2006; Symes, 2009). This method consists of the following steps: (1) compute the *state variables*, i.e. the seismic wavefields obtained from the source by forward modeling; (2) compute the *adjoint source*, i.e. a calculation based on the OF and on the state variables; (3) compute the *adjoint state variables*, i.e. the seismic wavefields obtained from the adjoint source by backward modeling; (4) compute the *gradient* using the state and adjoint state variables.

The state variables relate the OF to the model parameters as a solution of the acoustic wave equation

$$\begin{bmatrix} \mathcal{L}\left(\mathbf{x},\omega,m\right) & 0 \\ 0 & \mathcal{L}^{*}\left(\mathbf{x},\omega,m\right) \end{bmatrix} \begin{bmatrix} u_s\left(\mathbf{e},\mathbf{x},\omega\right) \\ u_r\left(\mathbf{e},\mathbf{x},\omega\right) \end{bmatrix} = \begin{bmatrix} f_s\left(\mathbf{e},\mathbf{x},\omega\right) \\ f_r\left(\mathbf{e},\mathbf{x},\omega\right) \end{bmatrix} . \tag{1}$$

$\mathcal{L}$ and $\mathcal{L}^{*}$ are forward and adjoint frequency-domain wave operators, u_s and u_r are the simulated source and receiver wavefields, f_s and f_r are the source and recorded data, m are the model parameters, $\mathbf{e}$ is the experiment index, ω is the frequency, and $\mathbf{x}$ are the space coordinates $\{x, y, z\}$.

The OF is formulated to minimize image inconsistencies caused by the model errors

$$\mathcal{H} = \frac{1}{2}\| K_I\left(\mathbf{x}\right) P\left(\boldsymbol{\lambda}\right) r\left(\mathbf{x},\boldsymbol{\lambda}\right) \|^2_{\mathbf{x},\boldsymbol{\lambda}} , \tag{2}$$

and it is based on extended image

$$r\left(\mathbf{x},\boldsymbol{\lambda}\right) = \sum_{\mathbf{e}} \sum_{\omega} \overline{u_s\left(\mathbf{e},\mathbf{x}-\boldsymbol{\lambda},\omega\right)} u_r\left(\mathbf{e},\mathbf{x}+\boldsymbol{\lambda},\omega\right) \tag{3}$$

The mask operator $K_I\left(\mathbf{x}\right)$ restricts the evaluation of the OF to some locations in the image, and $P\left(\boldsymbol{\lambda}\right)$ is a penalty operator acting on the extended image to highlight defocusing, i.e. image inaccuracy. It is typically assumed that defocusing is only due to velocity error, such that for correct models images focus completely at $\boldsymbol{\lambda} = 0$. In this case, we can define $P\left(\boldsymbol{\lambda}\right) = |\boldsymbol{\lambda}|$, which is the differential semblance optimization (DSO) operator of Symes (2009). However, this penalty operator is not effective when poor illumination affects the image accuracy and leads to additional defocusing. The DSO operator simply translates all image defocusing into model updates, which is incorrect.

As alternative technique advocated in this paper is to capture the illumination effects in the penalty operator by making it image-dependent, as opposed to a prescribed penalty based on an assumption of perfect focusing. Then, we can compare the current extended images with this partially defocused image due to illumination, as opposed to an ideal image assumed by DSO. The challenge is to construct a template image that does not suffer from velocity errors, but merely from illumination distortions. One way

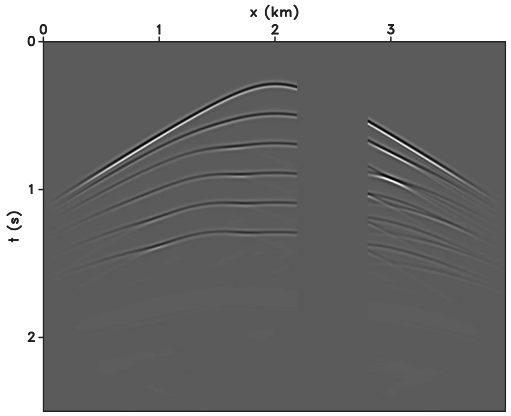

Figure 1: A shot gather for a source at $x = 2.0$ km showing the missing traces which simulate partial illumination due to an acquisition obstacle.

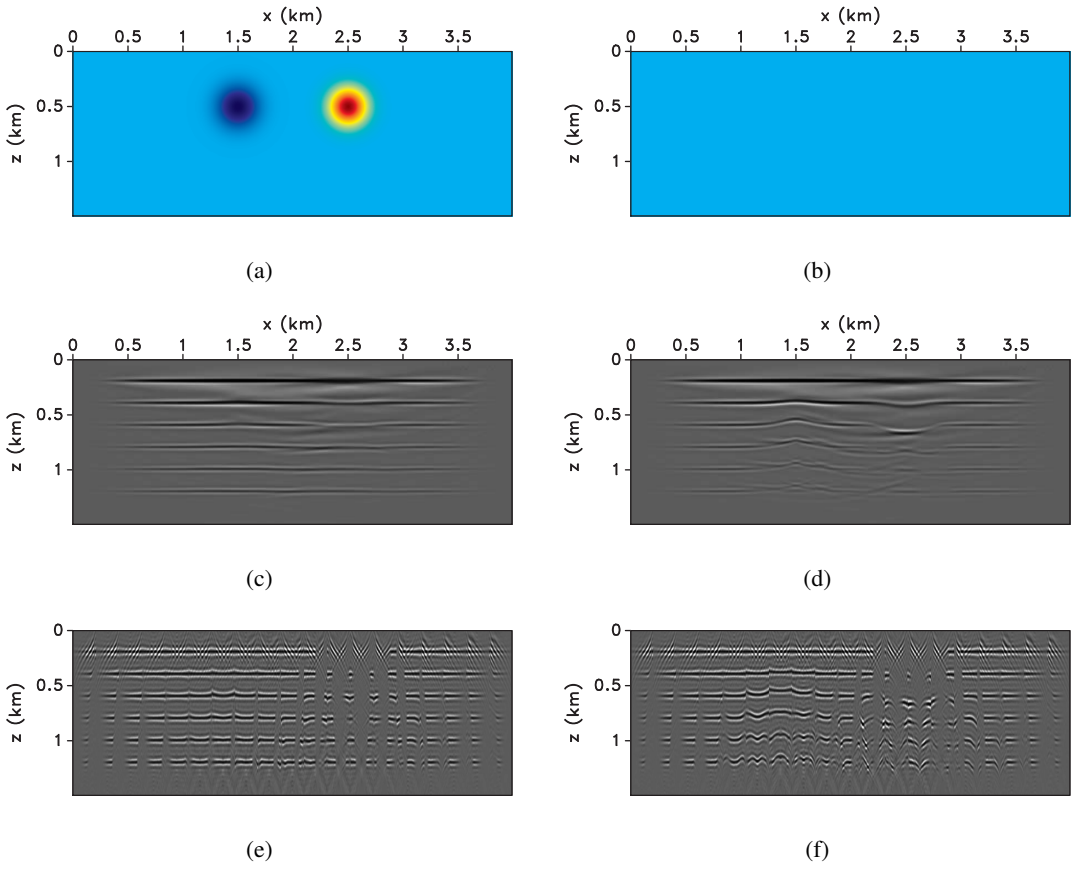

Figure 2: Velocity models (a and b), conventional images (c and d), and angle gathers (e and f) for the correct and starting models, respectively.

to achieve this goal is by modeling and migration in the current model starting from an ideal image based on the current image and velocity model. The resulting template image captures all illumination effects, but it is not subject to velocity error. We define the penalty operator based on the inverse energy of this template image, thus generalizing the DSO technique which assumes that all image energy concentrates at $\boldsymbol{\lambda} = 0$.

Using the penalty function, we can derive the adjoint sources used to model the adjoint state variables as the derivatives of $\mathcal{H}$ (equation 2) with respect to the state variables u_s and u_r, respectively:

$$\begin{bmatrix} g_s\left(\mathbf{e},\mathbf{x},\omega\right) \\ g_r\left(\mathbf{e},\mathbf{x},\omega\right) \end{bmatrix} = \begin{bmatrix} K_I\left(\mathbf{x}\right)\overline{K_I\left(\mathbf{x}\right)}\sum\limits_{\boldsymbol{\lambda}} P\left(\boldsymbol{\lambda}\right)\overline{P\left(\boldsymbol{\lambda}\right)r\left(\boldsymbol{\lambda}\right)}u_r\left(\mathbf{e},\mathbf{x}+\boldsymbol{\lambda},\omega\right) \\ K_I\left(\mathbf{x}\right)\overline{K_I\left(\mathbf{x}\right)}\sum\limits_{\boldsymbol{\lambda}} P\left(\boldsymbol{\lambda}\right)\overline{P\left(\boldsymbol{\lambda}\right)}r\left(\boldsymbol{\lambda}\right)u_s\left(\mathbf{e},\mathbf{x}-\boldsymbol{\lambda},\omega\right) \end{bmatrix}. \tag{4}$$

The adjoint state variable a_s and a_r are the wavefields obtained by backward and forward modeling using the corresponding adjoint sources:

$$\begin{bmatrix} \mathcal{L}^* \left(\mathbf{x}, \omega, m\right) & 0 \\ 0 & \mathcal{L} \left(\mathbf{x}, \omega, m\right) \end{bmatrix} \begin{bmatrix} a_s \left(\mathbf{e}, \mathbf{x}, \omega\right) \\ a_r \left(\mathbf{e}, \mathbf{x}, \omega\right) \end{bmatrix} = \begin{bmatrix} g_s \left(\mathbf{e}, \mathbf{x}, \omega\right) \\ g_r \left(\mathbf{e}, \mathbf{x}, \omega\right) \end{bmatrix} , \tag{5}$$

and the gradient is the correlation of the state and adjoint-state variables:

$$\frac{\partial \mathcal{H}}{\partial m} = \sum_{\mathbf{e}} \sum_{\omega} \frac{\partial \mathcal{L}}{\partial m} \left(u_s \left(\mathbf{e}, \mathbf{x}, \omega\right) \overline{a_s \left(\mathbf{e}, \mathbf{x}, \omega\right)} + u_r \left(\mathbf{e}, \mathbf{x}, \omega\right) \overline{a_r \left(\mathbf{e}, \mathbf{x}, \omega\right)} \right) . \tag{6}$$

The model is then updated using gradient line search aimed at minimizing the OF given by equation 2.

Example

We illustrate our new penalty operator with the model shown in Figures 2(a) and 2(c). The model includes high and low Gaussian anomalies at $x = 1.5$ km and at $x = 2.5$ km. We consider 5 horizontal interfaces and use finite-difference modeling to generate 73 shots like the one shown in Figure 1. We use the data gap between $x = 2.25 - 2.75$ km to simulate imaging illumination gaps. The migrated images and angle gathers for the true and starting models are plotted in Figures 2(c)-2(f). We invert using the DSO and illumination penalty operators, shown in Figures 3(a)-3(b), respectively. The updated model after 30 nonlinear iteration are shown in Figures 3(c) and 3(d). The migrated images, space-lag and angle gathers for the two updated models are shown in Figures 3(e)-3(j). The result obtained from the illumination-based penalty is significantly better than the DSO result. Although the space-lag gathers obtained from the DSO penalty are more focused at $\boldsymbol{\lambda} = 0$, the inversion fails to produce the correct answer since the penalty does not take the uneven illumination into account, thus translating illumination defocusing into velocity updates. In contrast, the space-lag gathers for the illumination-based penalty have residual moveout, which is consistent with the subsurface illumination, and the image is closer to the correct answer. The angle gathers also show the improved image quality of the model obtained with the illumination-based penalty.

Conclusions

Wavefield tomography using differential semblance optimization make an implicit assumption of perfect subsurface illumination and infinite bandwidth data. The penalty operator used in the definition of the objective function corresponds to this ideal case, thus this technique fails to produce robust results in areas of poor illumination. This problem can be addressed with the definition of an improved penalty function which uses the actual migrated image based on the current acquisition and velocity model. Replacing the conventional DSO penalty operator with one taking the actual subsurface illumination into account increases the robustness and accuracy of WT, especially in poorly illuminated areas, e.g. sub-salt.

Acknowledgments

We acknowledge the sponsors of the Center for Wave Phenomena at Colorado School of Mines. The reproducible numeric examples use the Madagascar open-source package (http://www.reproducibility.org).

REFERENCES

Plessix, R.-E., 2006, A review of the adjoint state method for computing the gradient of a functional with geophysical applications: Geophysical Journal International, **167**, 495–503.

———, 2009, Three-dimensional frequency-domain full-waveform inversion with an iterative solver: Geophysics, **74**, WCC53–WCC61.

Pratt, R. G., 1999, Seismic waveform inversion in the frequency domain, Part 1: Theory and verification in a physical scale model: Geophysics, **64**, 888–901.

Sirgue, L., and R. Pratt, 2004, Efficient waveform inversion and imaging: A strategy for selecting temporal frequencies: Geophysics, **69**, 231–248.

Symes, W., 2009, Migration velocity analysis and waveform inversion: Geophysical Prospecting, **56**, 765–790.

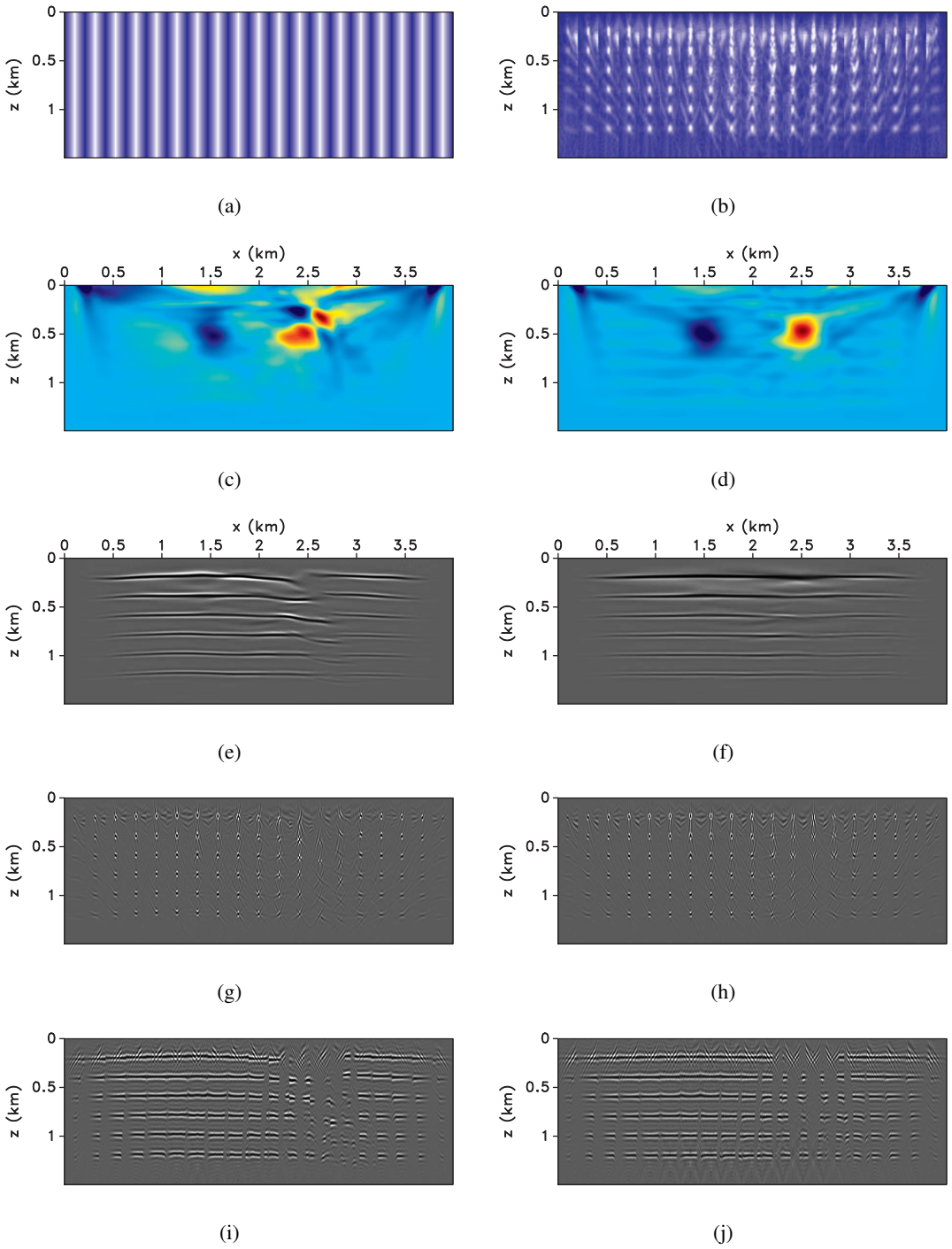

Figure 3: Penalty operators (a and b), velocity models (c and d), conventional images (e and f), space-lag gathers (g and h) and angle gathers (i and j) for inversion using the DSO and the illumination-based penalties, respectively. In panels (a) and (b), the penalty values increase from light to dark colors.

Tarantola, A., 1984, Inversion of seismic reflection data in the acoustic approximation: Geophysics, **49**, 1259–1266.

Vigh, D., and E. W. Starr, 2008, 3D prestack plane-wave, full-waveform inversion: Geophysics, **73**, VE135–VE144.

Woodward, M. J., 1992, Wave-equation tomography: Geophysics, **57**, 15–26.

Yang, T., and P. Sava, 2011, Waveform inversion in the image domain: Presented at the 73rd Mtg., Abstracts, Eur. Assoc. Expl. Geophys.